City Research Online

City, University of London Institutional Repository

Design of Power-Splitter With Selectable Splitting-ratio Using Angled and Cascaded MMI-coupler

Weifeng Jiang and B. M. Azizur Rahman, *Fellow, IEEE, Fellow, OSA, Fellow, SPIE*

Abstract—**A concept of power splitter with selectable splitting-ratios is proposed based on two multimode interference (MMI) sections connected by a phase-shifting region, in which phase-matching conditions can be fulfilled by using a simple angled section or alternatively using matched phase-shifters. The design example of an asymmetrical splitter (10 : 90) is optimized by using the transfer matrix method and three-dimensional full-vectorial beam propagation method. The numerical results reveal that a simple 1.2° angled section can yield a 10 : 90 splitter with an insertion loss of 0.74 dB and a total length of 192 μm. It is also shown that, for the cascaded MMI couplers based splitter, a more compact length of 58 μm with a lower insertion loss of 0.41 dB can be achieved. The fabrication tolerances are also investigated for the proposed asymmetrical power splitter.**

Index Terms—**Silicon photonics, power splitter, multimode interference.**

I. INTRODUCTION

S ILICON photonics show excellent potential to achieve compact photonic integrated circuits (PICs) exploiting the complementary metal-oxide-semiconductor (CMOS) compatible process and high-index contrast silicon waveguides [1],[2]. Optical power splitters are indispensable devices for building PICs based systems [3],[4]. Although traditionally uniform power splitters have been widely studied and developed, it is essential to explore an asymmetrical power splitter with unequal splitting ratios for many applications, such as for tapping optical signals [5], power equalizers [6], ring lasers [7], non-uniform Mach-Zehnder interferometers (MZIs) [8] and tunable optical filters using a ladder-type structure [9].

Various approaches have been reported to achieve an asymmetrical power splitter, including an asymmetrical Y-branch [10], a T-junction structure [11], a photonic crystal power splitter [12], a circular-to-rectangular polymer-fiber converter [13], an asymmetrical MZI [14], an asymmetrical coupler with phase control sections [15], and several kinds of multimode-interference (MMI) based power splitters [16]. Among these approaches, MMI structures have been widely

used to realize asymmetrical power splitters, owing to their compact footprints, better fabrication tolerances, low-loss, and broad bandwidth [17-20]. However, a traditional 2×2 MMIs based power splitter can only provide several discrete splitting ratios of 100 : 0, 85 : 15, 72 : 28, and 50 : 50 by choosing appropriate input-positions [21]. Deng *et al.* have reported a design for arbitrary power splitting ratio of a 1×2 MMI splitter by adjusting a notch in the MMI section [22]. To overcome some of the shortcomings, several approaches such as the electro-optic (EO) [23] or thermo-optic (TO) [24] effect based MMIs, hybrid plasmonic waveguide based MMI [25], butterfly-MMI [26], bent MMI [27],[28], asymmetric MMI [29] and cascaded MMIs (CMMIs) with phase shifters [30] have been proposed to address these limitations. One approach could be the use of the EO or TO effect based MMIs. A tunable power splitter has been demonstrated based on an EO-MMI, in which a 6 dB tuning range was experimentally obtained by applying a driving voltage of 54 V on the top of the multimode section [31]. Although this EO-MMI can provide asymmetrical power splitting ratios, it suffers from the free-carrier absorption and temperature-effects, which would induce a performance degradation and an increased propagation loss. In order to achieve a compact power splitter, a hybrid plasmonic waveguide based MMI with a metal cap has been proposed [32]. Two compact and asymmetrical power splitters with lengths of 650 nm and 900 nm of MMI sections are shown to provide splitting ratios in the ranges of 97.1 : 2.9 to 1.7 : 98.3 and 84 :16 to 16 : 84 through numerical simulations by using a 2×2 MMI structure and an asymmetric Y-branch, respectively [32]. Nevertheless, the fabrication-processes of these structures are complicated and the hybrid plasmonic waveguide may suffer from an increased propagation loss due to the metallic absorption. Another approach could be the use of a butterfly-MMI, which can achieve a compact and polarization-insensitive power splitter with a free selection of power splitting ratios [33]. However, the phase shifters based on a specific butterfly geometrical configuration need to be precisely controlled. Another approach could be the use of a bent MMI, in which a variable power splitter with a relaxed fabrication

Weifeng Jiang is with the College of Electronic and Optical Engineering, Nanjing University of Posts and Telecommunications, Nanjing 210023, China. (email: jwf@njupt.edu.cn).

B. M. Azizur Rahman is with the Department of Electrical and Electronic Engineering, City, University of London, Northampton Square, London EC1V OHB, UK. (email: B.M.A.Rahman@city.ac.uk).

tolerance can be obtained at angle = 0° and higher angles [34]. But, this bent-MMI based power splitter may suffer from the extra bending loss. Another approach could be the use of the CMMIs with or without phase shifters. By cascading three or four 2×2 MMI sections, nineteen different power splitting ratios can be yielded [35]. Both the wide bandwidth and large tolerance can be achieved based on these CMMIs without any phase shifter. Similarly, by cascading two 2×2 MMI sections, four different fixed splitting ratios (0.07, 0.64, 0.80, and 0.93) can be achieved [36]. In order to realize freely chosen power splitting ratio, several CMMIs with different phase shifters have been reported, in which phase shifters can be implemented based on the TO effect, connecting waveguides with unequal width/height/length or two taper waveguides between two MMI sections [37-40]. Nevertheless, the above reported asymmetrical splitters have a limited number of output ports of ≤ 3 (1×2, 2×2, or 1×3). Although a $1 \times M$ (more than 3 outputs) asymmetrical splitter can also be achieved by cascading several such splitters, but the fabrication-errors and footprints would simultaneously be increased significantly.

In this paper, we propose a concept of the power splitter with selectable splitting-ratios based on two MMI sections connected by a phase-shifting region, in which phase-matching conditions can be fulfilled by using simple angled structures or alternatively using matched phase-shifters. Any number of the outputs with selectable splitting-ratios can be directly yielded. All outputs are independent and the performances are mainly affected by the errors of the central isolated phase-shifting sections. An asymmetrical splitter (10 : 90) is optimized as an example via simple cascaded 1×10 and 9×1 MMI couplers. In this case, the proposed asymmetrical power splitter is optimized by using the transfer matrix method (TMM) and three-dimensional full-vectorial beam propagation method (3D-FV-BPM).
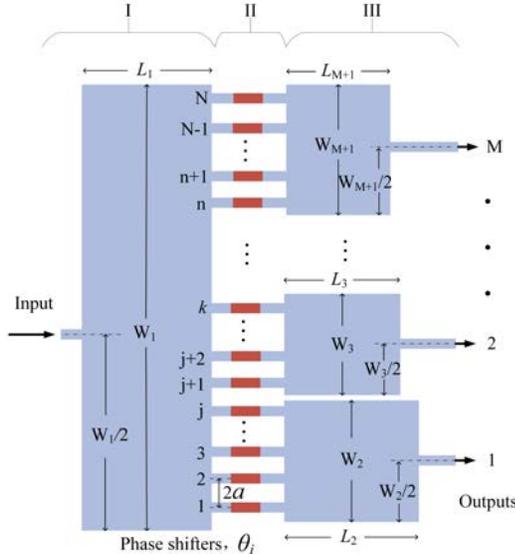
Fig. 1. Schematic diagram of the proposed power splitter with selectable splitting ratios.

II. Results

The schematic diagram of the proposed power splitter with

selectable splitting-ratios is shown in Fig. 1, which consists of three sections I, II and III. Section I is a uniform $1 \times N$ MMI-splitter with the size of $W_1 \times L_1$. The spacing between N self-images is $2a$. Section II is the phase-shifting region, which can be fulfilled by utilizing simple angled structures or alternatively matched phase-shifters, θ_i, ($i = 1, 2, 3, \ldots N$). In section III, there are M MMI-combiners with the sizes of the MMI waveguides of $W_2 \times L_2$, $W_3 \times L_3$, $\ldots$ and $W_{M+1} \times L_{M+1}$, respectively. The numbers of the inputs of these MM-combiners are set to be j, (k-j), $\ldots$ and (N-n+1), respectively. The configurations of the power splitter based on the proposed concept can be achieved as 1×2, 1×3, $\ldots$ and $1 \times M$. The selectable splitting-ratios are summarized in Table 1, where j, k, n, N, and M are any positive integers. For the example of N = 10, the splitting ratios of 1×2 splitters can be attained to be 10 : 90 , 20 : 80, 30 : 70, 40 : 60, and 50 : 50. For a 1×3 splitter, 36 different splitting-ratios can be realized for N = 10. Similarly, many other splitting-ratios can be obtained for any $1 \times M$ splitter. Furthermore, the unequal power splitting of $1 \times N$ MMI-splitter in section I can be achieved depending on the position of the input waveguide and then additional splitting-ratios can be obtained for $1 \times M$ splitters.

Table 1. Selectable splitting-ratios of the power splitters based on the proposed concept.

Output Channels $1 \times M$	Channels No.		Splitting Ratios at Outputs	Conditions
	j	k		
1×2	N-1	/	1 : N-1	$2 \leq j < N$
	j	N	(N-j) : j	
1×3	j	n-1	(N-n+1) : (n-1-j) : j	$j < n < N$ and $n \geq 3$
$1 \times M$	j	k	(N-n+1) : ... : (k-j) : j	$j < k < n \leq N$

The schematic of the asymmetrical power splitter (10 : 90) based on the cascaded 1×10 and 9×1 MMI couplers is shown in Fig. 2. An asymmetrical power splitter based on an angled MMI coupler is shown in Fig. 2(a), consisting of a 1×10 MMI splitter, a 9×1 MMI combiner, a phase-shifting region, and a straight output access waveguide. An equivalent model of Fig. 2(a) but also an alternate design is illustrated in Fig. 2(b), incorporating two CMMI couplers, which consists of a 1×10 MMI splitter, a 9×1 MMI combiner, a phase-shifting region with 9 arms and combined phase shifters, and an output access waveguide. The passive phase shifters are shown by red regions and can be adjusted by changing the width of the waveguide. In this work, these two structures are on the silicon-on-insulator (SOI) platform with a standard silicon thickness of 220 nm. An upper silica cladding is added to avoid the external environment influence. The width and length of the 1×10 MMI splitter are denoted by W_1 and L_1, respectively. The width and length of the 9×1 MMI combiner are denoted by W_2 and L_2, respectively. The width of input and output access waveguides is $w = 400$ nm for the single-mode operation. The input and output access waveguides are placed at the centers of the 1×10 MMI splitter and 9×1 MMI combiner, respectively. In order to reduce the loss, the output access waveguide is widened to a width of w_t by using a taper with a length of L_t. The output access

waveguide, O_1, is of a spacing, a, to the upper edge of the 1×10 MMI splitter. It can be observed from Fig. 2(a) that the angle between the output plane of the 1×10 MMI splitter and the input plane of the 9×1 MMI combiner is denoted by θ, which can provide a progressive phase shifting for 9 different channels. For the CMMI-coupler shown in Fig. 2(b), an input field is distributed at the output plane of the 1×10 MMI splitter in the form of 10 self-images that have the same spacing of $2a$, equal magnitude, and different phases. 9 arms are of the same length and with phase shifters, in which phases of 9 branches can be changed as required to satisfy phase-matching conditions between the 1×10 MMI splitter and 9×1 MMI combiner for different channels simultaneously. The amounts of phase variations are denoted by θ_i, $i = 1, 2, \ldots, 9$. The arms, k at the input plane of the 9×1 MMI combiner are also with the same spacing of $2a$. In this paper, the angled MMI-coupler and the CMMI-coupler based asymmetrical power splitters are studied by using the TMM and 3D-BPM sequentially.

(a)

(b)
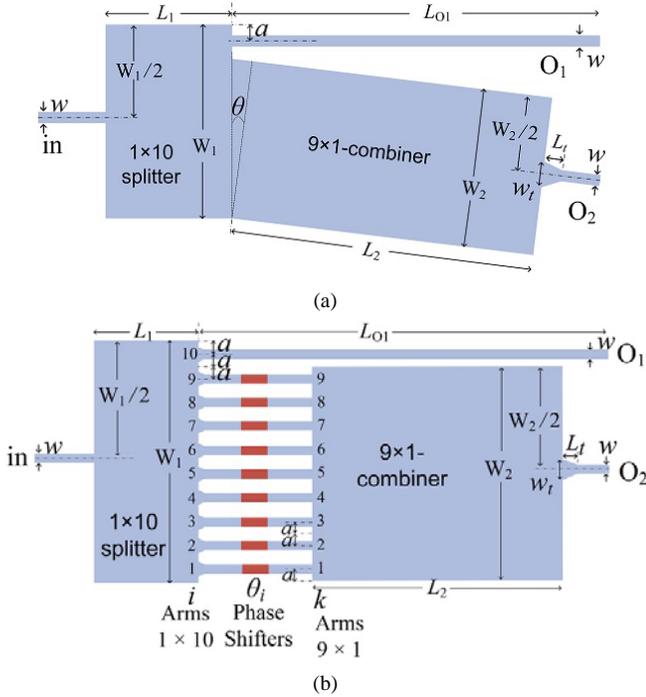
Fig. 2. Schematic of asymmetrical power splitter (10 : 90) based on CMMI couplers. (a) Angled MMI-coupler. (b) CMMI couplers with phase shifters. These two structures are corresponding to the first ($M = 1$) and second ($M = 2$) 9-fold images distances.

Before the optimal design of the asymmetrical power splitter, it is necessary to derive the phases of the 1×10 MMI splitter and 9×1 MMI combiner, respectively. For a uniform $1 \times N$ coupler with an input field at the center, output phases are given by the following equations [21]:

$$\Phi_i^M = \varphi_n^M + \frac{M\pi}{N}(p-1)(N-p) \tag{1}$$

$$\varphi_n^M = -\beta_n L_n^M - \frac{M\pi}{4N}(N^2 - 3N + 1) \tag{2}$$

where M is a multiple occurrence of N self-images at different device lengths. Here, p is the numbering of the nonzero outputs; φ_n^M is a constant phase shift depending on the MMI length and

β_n is the propagation constant of the fundamental mode. The subscripts, $n = 1$ and 2 are corresponded to the propagation constants of the fundamental modes for the 1×10 splitter and 9×1 combiner MMI waveguides, respectively.

The overall transfer matrix of this asymmetrical power splitter based on both structures shown in Figs. 2(a) and 2(b) is given by

$$\begin{bmatrix} E_{O2} \\ 0 \\ 0 \\ 0 \\ 0 \\ 0 \\ 0 \\ 0 \\ 0 \\ 0 \end{bmatrix} = [T_2] \bullet [S] \bullet [T_1^*] \bullet \begin{bmatrix} E_{in} \\ 0 \\ 0 \\ 0 \\ 0 \\ 0 \\ 0 \\ 0 \\ 0 \\ 0 \end{bmatrix} \tag{3}$$

where E_{in} and E_{O2} are the complex optical electric field amplitudes at the input port and output port O_2, respectively. $[T_1^*]$ represents the transfer matrix of the 1×10 MMI splitter for arms $i = 1, 2, \ldots, 9$. $[S]$ and $[T_2]$ indicate the transfer matrices for the phase shifters and the 9×1 MMI combiner.

For a uniform 1×10 MMI splitter, the transfer matrix at first 10-fold images distance, $[T_1^*]$ for arms $i = 1, 2, \ldots, 9$, can be obtained from equations (1) and (2), as below

$$[T_1^{1*}] = \frac{e^{j\varphi_1^1}}{\sqrt{10}} \bullet \begin{bmatrix} 1 & 0 & 0 & 0 & 0 & 0 & 0 & 0 & 0 \\ e^{j\bullet\frac{4\pi}{5}} & 0 & 0 & 0 & 0 & 0 & 0 & 0 & 0 \\ e^{j\bullet\frac{7\pi}{5}} & 0 & 0 & 0 & 0 & 0 & 0 & 0 & 0 \\ e^{j\bullet\frac{9\pi}{5}} & 0 & 0 & 0 & 0 & 0 & 0 & 0 & 0 \\ e^{j\bullet 2\pi} & 0 & 0 & 0 & 0 & 0 & 0 & 0 & 0 \\ e^{j\bullet 2\pi} & 0 & 0 & 0 & 0 & 0 & 0 & 0 & 0 \\ e^{j\bullet\frac{9\pi}{5}} & 0 & 0 & 0 & 0 & 0 & 0 & 0 & 0 \\ e^{j\bullet\frac{7\pi}{5}} & 0 & 0 & 0 & 0 & 0 & 0 & 0 & 0 \\ e^{j\bullet\frac{4\pi}{5}} & 0 & 0 & 0 & 0 & 0 & 0 & 0 & 0 \end{bmatrix} \tag{4}$$

It can be noted from Fig. 2(b) that the transfer matrix for the phase shifters, $[S]$ can be given by

$$[S] = \begin{bmatrix} e^{j\bullet\theta_1} & 0 & 0 & 0 & 0 & 0 & 0 & 0 & 0 \\ 0 & e^{j\bullet\theta_2} & 0 & 0 & 0 & 0 & 0 & 0 & 0 \\ 0 & 0 & e^{j\bullet\theta_3} & 0 & 0 & 0 & 0 & 0 & 0 \\ 0 & 0 & 0 & e^{j\bullet\theta_4} & 0 & 0 & 0 & 0 & 0 \\ 0 & 0 & 0 & 0 & e^{j\bullet\theta_5} & 0 & 0 & 0 & 0 \\ 0 & 0 & 0 & 0 & 0 & e^{j\bullet\theta_6} & 0 & 0 & 0 \\ 0 & 0 & 0 & 0 & 0 & 0 & e^{j\bullet\theta_7} & 0 & 0 \\ 0 & 0 & 0 & 0 & 0 & 0 & 0 & e^{j\bullet\theta_8} & 0 \\ 0 & 0 & 0 & 0 & 0 & 0 & 0 & 0 & e^{j\bullet\theta_9} \end{bmatrix} \tag{5}$$

A. Design Analysis at $M = 1$

There are two possible options for the transfer matrix of the 9×1 MMI combiner, corresponding to the first ($M = 1$) and second ($M = 2$) 9-fold images distances, which also correspond to the asymmetrical power splitter based on the angled MMI-coupler and the CMMI-coupler, respectively. Next, their

principles will be studied in detailed. First, we consider the transfer matrix at first 9-fold images distance for the 9×1 MMI combiner. The transfer matrix at first 9-fold images distance, $[T_2^1]$ is obtained by using equations (1) and (2) and given by

$$[T_2^1] = \frac{e^{j\varphi_2^1}}{3} \bullet \begin{bmatrix} 1 & e^{j\bullet\frac{7\pi}{9}} & e^{j\bullet\frac{4\pi}{3}} & e^{j\bullet\frac{5\pi}{3}} & e^{j\bullet\frac{16\pi}{9}} & e^{j\bullet\frac{5\pi}{3}} & e^{j\bullet\frac{4\pi}{3}} & e^{j\bullet\frac{7\pi}{9}} & 1 \\ 0 & 0 & 0 & 0 & 0 & 0 & 0 & 0 & 0 \\ 0 & 0 & 0 & 0 & 0 & 0 & 0 & 0 & 0 \\ 0 & 0 & 0 & 0 & 0 & 0 & 0 & 0 & 0 \\ 0 & 0 & 0 & 0 & 0 & 0 & 0 & 0 & 0 \\ 0 & 0 & 0 & 0 & 0 & 0 & 0 & 0 & 0 \\ 0 & 0 & 0 & 0 & 0 & 0 & 0 & 0 & 0 \\ 0 & 0 & 0 & 0 & 0 & 0 & 0 & 0 & 0 \\ 0 & 0 & 0 & 0 & 0 & 0 & 0 & 0 & 0 \end{bmatrix} \quad (6)$$

Considering the phase differences between the 1×10 MMI splitter and 9×1 MMI combiner, we can obtain the transfer matrix necessary for the phase shifters. The matrix for each phase shifter is given as below, in which the constant phase shift is not included.

$$\begin{bmatrix} e^{j\bullet\theta_1} \\ e^{j\bullet\theta_2} \\ e^{j\bullet\theta_3} \\ e^{j\bullet\theta_4} \\ e^{j\bullet\theta_5} \\ e^{j\bullet\theta_6} \\ e^{j\bullet\theta_7} \\ e^{j\bullet\theta_8} \\ e^{j\bullet\theta_9} \end{bmatrix} = \begin{bmatrix} 1 \\ e^{-j\bullet\frac{\pi}{45}} \\ e^{-j\bullet\frac{\pi}{15}} \\ e^{-j\bullet\frac{2\pi}{15}} \\ e^{-j\bullet\frac{2\pi}{9}} \\ e^{-j\bullet\frac{\pi}{3}} \\ e^{-j\bullet\frac{7\pi}{15}} \\ e^{-j\bullet\frac{28\pi}{45}} \\ e^{-j\bullet\frac{4\pi}{5}} \end{bmatrix} \quad (7)$$
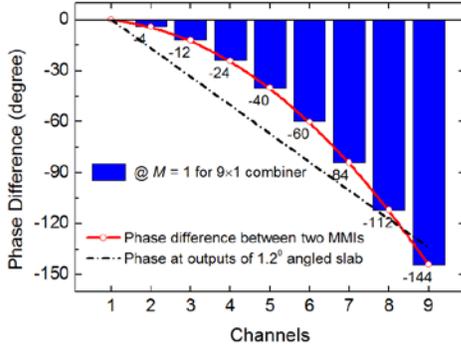
Fig. 3. Phase differences between 1×10-output plane and 9×1-input plane at $M = 1$. TMM was employed in the calculation.

In order to elaborate the pattern for the phase differences between the 1×10 MMI splitter and 9×1 MMI combiner, variations of the phase differences as a function of different channels are shown in Fig. 3. The phase differences of each channel are denoted by blue bars. The red solid line represents variations of the phase difference with the channel number. It can be noted that the phase difference is monotonically decreased with the increase of the channel number. Therefore, the phase shifting can be yielded via a quasi-triangle-shaped waveguide, which can approximately satisfy the phase-

matching condition between the output plane of the 1×10 MMI splitter and the input plane of the 9×1 MMI combiner. The phases at outputs of the 1.2° angled slab waveguide are shown by a black dashed-dotted line, which can be a linear approximation of the phase differences necessary between the output plane of the 1×10 MMI splitter and the input plane of the 9×1 MMI combiner. The reason for the choice of this angle, 1.2° will be discussed later in Fig. 4.

It can be noted from Fig. 2(a) that a triangle-shaped phase-shifting region can be obtained by using the angled MMI-coupler. An input field can be distributed at the output plane of the 1×10 MMI splitter in the form of 10 self-images with equal magnitude and different phases. The uppermost image, with 1/10 of the total power, is directly output through the access waveguide, O_1. The other 9 images propagate along the phase-shifting region and undergo different phase variations simultaneously. By adjusting the angle, θ, the amount of phase variations at the phase-shifting region can be optimized to approximately satisfy the phase-matching condition between the 1×10 MMI splitter and 9×1 MMI combiner. After propagating through the 9×1 MMI combiner, other 9 images are combined at the output port O_2. Therefore, an asymmetrical power splitter (10 : 90) can be produced by using an angled MMI-coupler, in which 1/10 and 9/10 of the total power are output at ports O_1 and O_2, respectively.

For the optimal design of the angled MMI-coupler, a uniform 1×10 MMI splitter needs to be studied firstly. In general, the spacing, $2a$, between each pair of the output images should be as short as possible to minimize the size of the MMI coupler. On the contrary, a smaller spacing can introduce a higher crosstalk, which also be limited by the lithographic process. In this case, the spacing, $2a = 1$ μm, is chosen to balance the size of the coupler and the crosstalk. Considering the 1×10 MMI structure shown in Fig. 2, the width of the 1×10 MMI splitter can be given as $W_1 = 10$ μm. For this 1×10 MMI splitter, the length, L_1 can be approximately given by $L_1 = 3L_\pi / 40$, where L_π is the beat length of the splitter, its approximate value can be obtained from [41]

$$L_\pi = \frac{\pi}{\beta_0 - \beta_1} \approx \frac{4N_{eff}W_e^2}{3\lambda} \quad (8)$$

where β_0 and β_1 are the propagation constants of the fundamental and first-order modes of the 1×10 MMI splitter, respectively. N_{eff} and W_e are the effective index and effective width of the multimode waveguide, respectively. The effective width, W_e can be calculated using an approximate [41]:

$$W_e = W_M + \left(\frac{\lambda}{\pi}\right)\left(\frac{n_c}{n_r}\right)^{2\sigma}\left(n_r^2 - n_c^2\right)^{-(1/2)} \quad (9)$$

where $\sigma = 0$ for the quasi-TE mode; $\sigma = 1$ for the quasi-TM mode; W_M is the width of the multimode waveguide. Here, n_c and n_r are the refractive indices of the cladding and core, respectively. However, we can state that we have calculated the exact value of the L_π from the accurate values of the propagation constants obtained from the vector mode solver.

In this case, the optimization of the proposed splitter is

studied by using the 3D-FV-BPM. The device is designed for the quasi-TE polarization. The refractive indices of the silicon and silica are taken as 3.47548 and 1.46, respectively at the operating wavelength of 1550 nm. The optimized length of the 1×10 MMI splitter is calculated as $L_1 = 23.5$ μm. According to the spacing between 9 images at the output plane of the 1×10 MMI splitter, the width of the 9×1 MMI combiner is chosen to be $W_2 = 9$ μm. In order to achieve the lowest insertion loss, the angle, θ, is adjusted to produce the best phase-matching between these two MMI couplers.
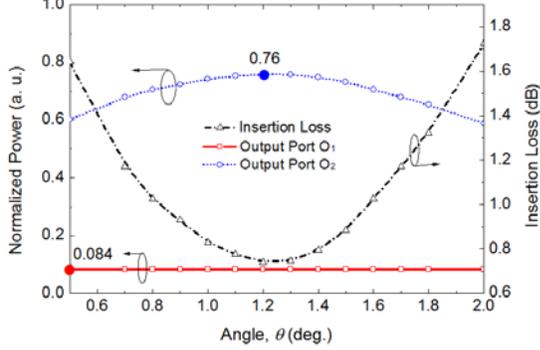
Fig. 4. Variations of the normalized power (left y-axis) and insertion loss (right y-axis) with the angle, θ. 3D-FV-BPM was employed in the calculation.

Variations of the normalized power (left y-axis) and insertion loss (right y-axis) with the angle are calculated by using a 3D-FV-BPM and shown in Fig. 4. The insertion loss is shown by a black dashed-dotted line. In order to reduce the loss, a taper with the size of $w_t = 1$ μm and $L_t = 2$ μm, is used for the output access waveguide O_2. A reasonable high transmission of 98.2% can be achieved for this taper. The normalized power at port O_1, shown by a red solid line, does not depend on θ, and its value is 0.084. This can be explained by the fact that the power at port O_1 is directly output from the 1×10 MMI splitter, which does not affect by variations of the angle. The slight reduction from its ideal value of 0.10 is due to abrupt junctions, and this loss can be reduced by using a tapered section. By using a 2 μm long tapered section, the addition loss of 0.016 can be reduced to only 0.002. The normalized power at port O_2, shown by a blue dotted line, increases with the increase of the angle from $\theta = 0.5°$ to $\theta = 1.2°$, reaches its maximum value at angle, $\theta = 1.2°$, and then power at port O_2 decreases. The maximum value of O_1 at $\theta = 1.2°$ is 0.76 shown by a blue dot in Fig. 4. It can also be noted that the insertion loss decreases with the increase of the angle from $\theta = 0.5°$ to $1.2°$, reaches its minimum value of 0.74 dB at angle, $\theta = 1.2°$, and subsequently from $\theta = 1.2°$ to $2.0°$, the insertion loss increases with the increase of the angle. Therefore, the optimal angle for the asymmetrical power splitter (10 : 90) is chosen to be $\theta = 1.2°$.
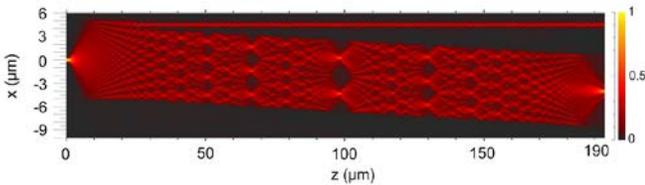
Fig. 5. Field distribution along the z-direction for asymmetrical power splitter (10 : 90) based on angled MMI-coupler. 3D-FV-BPM was employed in the calculation.

The field profile along the z-direction for the asymmetrical power splitter (10 : 90) based on an angled MMI coupler is calculated by using the 3D-FV-BPM and shown in Fig. 5. It can be observed that one image of the 1×10 MMI splitter is directly output at port O_1. Other 9 images are phase-adjusted to form the input images of the 9×1 MMI combiner at the first 9-fold images distance and then propagate through the combiner to give a 1-fold image based on the self-imaging. As stated earlier in Fig. 3, the dashed-dotted straight line is a linear approximation of optimal phase differences between two couplers for the best O_2 output. But, it can be noted from Fig. 5 that the performance is good enough to achieve a 10 : 90 power splitter. However, the total length of the asymmetrical power splitter is 192 μm. The length of the first and second MMI couplers are 23.5 μm and 163 μm, respectively. It can also be noted from Fig. 5 that the length of the 9×1 MMI combiner could be dramatically shortened by replacing the phases at $M = 1$ with those at $M = 2$, corresponding the second 9-fold images distance, but require a different phase compensation.

B. Design Analysis for $M = 2$

In order to achieve a more compact splitter, we consider the phase matching between the 1×10 MMI splitter and 9×1 MMI combiner at the second 9-fold images distance. According to equations (1) and (2), the transfer matrix at the second 9-fold images distance, $[T_2^2]$ is given by

$$[T_2^2] = \frac{e^{j\varphi_2^2}}{3} \bullet \begin{bmatrix} 1 & e^{j \bullet \frac{14\pi}{9}} & e^{j \bullet \frac{8\pi}{3}} & e^{j \bullet \frac{10\pi}{3}} & e^{j \bullet \frac{32\pi}{9}} & e^{j \bullet \frac{10\pi}{3}} & e^{j \bullet \frac{8\pi}{3}} & e^{j \bullet \frac{14\pi}{9}} & 1 \\ 0 & 0 & 0 & 0 & 0 & 0 & 0 & 0 & 0 \\ 0 & 0 & 0 & 0 & 0 & 0 & 0 & 0 & 0 \\ 0 & 0 & 0 & 0 & 0 & 0 & 0 & 0 & 0 \\ 0 & 0 & 0 & 0 & 0 & 0 & 0 & 0 & 0 \\ 0 & 0 & 0 & 0 & 0 & 0 & 0 & 0 & 0 \\ 0 & 0 & 0 & 0 & 0 & 0 & 0 & 0 & 0 \\ 0 & 0 & 0 & 0 & 0 & 0 & 0 & 0 & 0 \\ 0 & 0 & 0 & 0 & 0 & 0 & 0 & 0 & 0 \end{bmatrix} \quad (10)$$

Considering phase differences between the 1×10 MMI splitter and 9×1 MMI combiner at the second 9-fold images distance, we can obtain the transfer matrix for phase shifters from equations (4) and (10). The matrix shown here after excluding the constant phase shift for each phase shifter is given by

$$\begin{bmatrix} e^{j \bullet \theta_1} \\ e^{j \bullet \theta_2} \\ e^{j \bullet \theta_3} \\ e^{j \bullet \theta_4} \\ e^{j \bullet \theta_5} \\ e^{j \bullet \theta_6} \\ e^{j \bullet \theta_7} \\ e^{j \bullet \theta_8} \\ e^{j \bullet \theta_9} \end{bmatrix} = \begin{bmatrix} 1 \\ e^{j \bullet \frac{34\pi}{45}} \\ e^{j \bullet \frac{19\pi}{15}} \\ e^{j \bullet \frac{23\pi}{15}} \\ e^{j \bullet \frac{14\pi}{9}} \\ e^{j \bullet \frac{4\pi}{3}} \\ e^{j \bullet \frac{13\pi}{15}} \\ e^{j \bullet \frac{7\pi}{45}} \\ e^{-j \bullet \frac{4\pi}{5}} \end{bmatrix} \quad (11)$$

For the second 9-fold images distance of the 9×1 MMI combiner, variations of the phase differences with the channel

numbers are shown in Fig. 6. The phase differences for each channel are denoted by the red bars. With the increase of the channel number, the variation of the phase difference is expected to increase or decrease monotonically, but here, it can be noted from Fig. 6 that the phase differences of channels 3, 4, 5, 6, and 9 subtract $\pm 2\pi$ to minimize the amount of phase variations, respectively. Therefore, it is impossible to satisfy the phase-matching condition between two MMI couplers by using a sample angled structure as shown in Fig. 2(a).
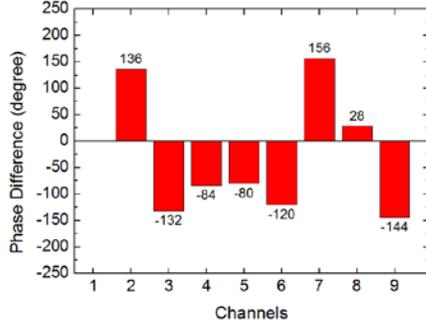
Fig. 6. Phase differences between the 1st and other ports when 1×10-output ports is connected to the 9×1-input ports with imaging, $M = 2$. TMM was employed in the calculation.

In order to obtain the phase shifting shown in Fig. 6, the CMMI-coupler is introduced to achieve an asymmetrical power splitter (10 : 90). The schematic diagram of the CMMI-coupler based asymmetrical power splitter is shown in Fig. 2(b). An input field is firstly distributed to 10 self-images with equal magnitude and different phases at the output plane of the 1×10 MMI splitter. The 10th image is directly output to the access waveguide, O_1. The 1st - 9th images propagate through 9 access waveguides of the same length between two MMI couplers. The phase shifters are located in the 9 connecting waveguides and can provide the necessary phase-matching conditions for different channels simultaneously. The phases of the fields propagating through the 9 connecting waveguides can be shifted by an amount of θ_i. After obtaining the necessary phase matching, the 9 images can be combined to 1-fold image. The effective propagation constants of the phase shifters can be adjusted by changing the etch-depth, etch-width or length of the shifters. In this case, we consider the variations of the etch-width to obtain the necessary phase shifting, in which no additional masking or processing step is needed. The amount of the phase shifting, θ_i, can be calculated by using $\theta_i = \Delta\beta_{psi}L_{psi}$, where $\Delta\beta_{psi}$ is the difference of propagation constants between the waveguide with the width of 400 nm and the phase shifter, θ_i. L_{psi} is the length of the phase shifter of the ith channel. In order to minimize the excess loss, widths of the phase shifters are set to either $W_{s1} = 420$ nm or $W_{s2} = 380$ nm for the positive or negative phase differences needed, respectively. 400 nm is the width of the waveguide which is taken as reference. The propagation constants are 8.797, 9.048, and 9.269 rad/μm for the waveguides with widths of 380, 400, and 420 nm, respectively. Subsequently, the lengths of phase shifters, θ_1, to θ_9, are calculated to be 0, 10.78, 9.21, 5.86, 5.58, 8.37, 12.37, 2.22, and 10.05 μm, according to the phase differences as shown in Fig. 6. The additional losses of the signal propagating through the phase shifters, θ_7 and θ_9, are only 0.0026 and 0.0045

dB, which correspond to the maximum lengths of $W_{s1} = 420$ nm and $W_{s2} = 380$ nm, respectively.
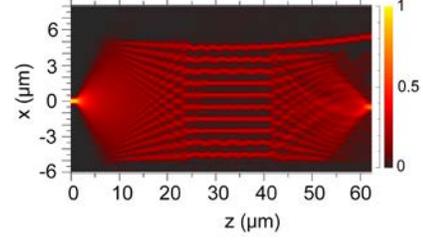
Fig. 7. Field distribution along the z-direction for asymmetrical power splitter (10 : 90) based on the CMMI-coupler at $M = 2$. 3D-FV-BPM was employed in the calculation.

The field profile along the z-direction for the asymmetrical power splitter (10 : 90) based on the CMMI-coupler is calculated by using the 3D-FV-BPM and shown in Fig. 7. It can be observed that one image of the 1×10 MMI splitter is directly output at port O_1. Other 9 images are phase-matched with input ports of the 9×1 MMI combiner at the second 9-fold images distance and then propagate through the combiner to give a 1-fold image. Thus, a compact asymmetrical-power splitter with a length of 58 μm can be achieved with an insertion loss of 0.41 dB. The length of the first and second MMI couplers are 23.5 μm and 21.3 μm, respectively.

Next, the output 1D E_x field shapes at port O_2 are shown in Fig. 8 for three different structures based asymmetrical power splitters. The output E_x field shapes of the CMMI-coupler based asymmetrical power splitter are shown by a red dotted line and a blue solid line for the phase matching at $M = 1$ and $M = 2$, respectively. The output E_x field shape of the angled MMI-coupler based asymmetrical power splitter is shown by a black dashed-dotted line for the phase matching at $M = 1$. The locations of the peak shifts along the x-direction for the angled design, as in these cases, the change in the axis of the 9×1 section shifts the positions of the output port along the x-direction. By comparing the phase matching at $M = 1$ and $M = 2$, it can be noted from Fig. 8 that the side-lobes can be significantly suppressed by using the CMMI-coupler at $M = 2$, which are corresponded to the phase matching between the 1×10 MMI splitter and the second 9-fold images distance of the 9×1 MMI combiner. It can also be noted that the amplitudes of the CMMI-coupler are greater than that of the angled MMI coupler based asymmetrical power splitter. This can be explained by that fact that the CMMI-coupler can provide a more accurate phase-shifting compared to a linear average compensation provided by an angled MMI-coupler.
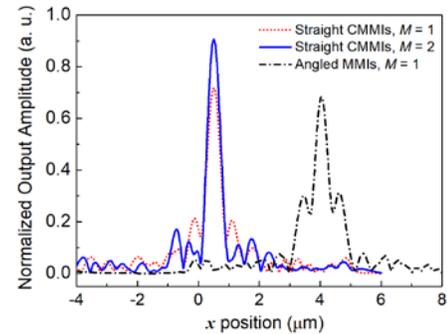
Fig. 8. Variations of normalized output amplitudes of the E_x field with x position.

3D-FV-BPM was employed in the calculation.

C. Bandwidth and Fabrication Tolerances

Variations of the insertion loss (left y-axis) and splitting ratio (right y-axis) with the wavelength are shown in Fig. 9 for the CMMI-coupler based power splitter at $M = 2$. The insertion loss and the splitting ratio are shown by a red dashed-dotted line and a blue solid line, respectively. It can be noted that the minimum insertion loss and its corresponding splitting ratio (O_2/O_1) are 0.41 dB and 8.99, respectively. The 1 dB bandwidth for the quasi-TE mode is nearly 95 nm. The deterioration of the splitting ratio is less than 2% over a bandwidth of 46 nm from 1509 nm to 1555 nm. The wavelength dependence for the angled MMI-coupler based asymmetrical power splitter was also calculated, but the detailed results are not presented here. Compared to the CMMI-coupler, the minimum loss of the angled MMI-coupler was 0.74 dB and its 1 dB bandwidth was slightly smaller, equal to 70 nm variation of the wavelength. With the ratio-change limit of 2%, the bandwidth of the angled MMI-coupler is calculated as 31 nm.
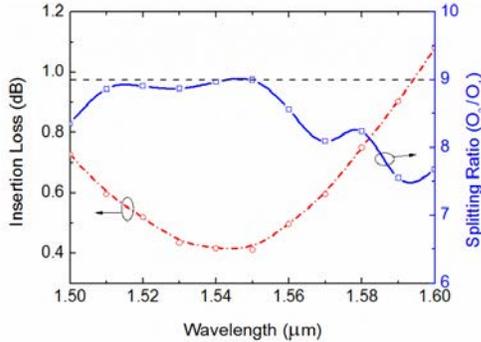
Fig. 9. Variations of the insertion loss (left y-axis) and splitting ratio (right y-axis) with the wavelength. 3D-FV-BPM was employed in the calculation. CMMI coupler-based layout taking $M = 2$.
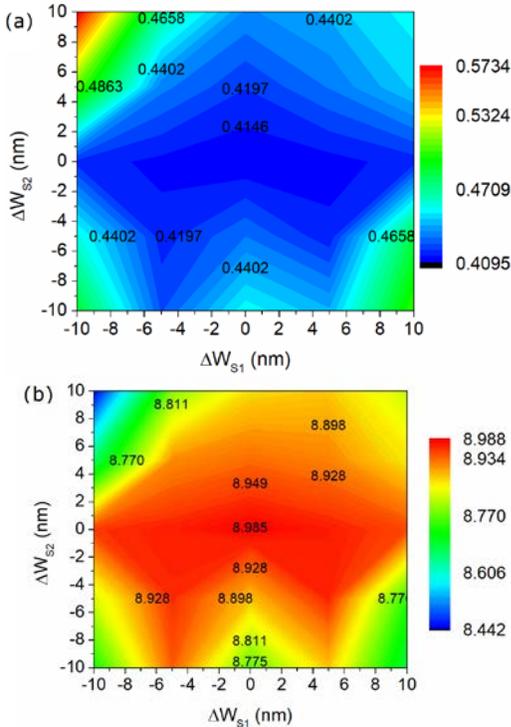
Fig. 10. Variations of the (a) insertion loss and (b) splitting ratio with the variations of W_{s1} and W_{s2}.

Although, CMOS technology is very mature, some changes can be expected from the optimized designed parameters. Variations of the insertion loss and splitting ratio with the simultaneous changes of the W_{s1} and W_{s2} are shown in Figs. 10(a) and 10(b), respectively for the CMMI-coupler based asymmetrical power splitter at $M = 2$. It can be noted from Fig. 10(a) that the insertion loss is increased with the increase in the changes of the W_{s1} or W_{s2}, which deteriorates the phase-matching condition. The insertion loss is increased by 0.164 dB for the $\pm$ 10 nm variations of both the W_{s1} and W_{s2}. It can also be noted from Fig. 10(b) that the splitting ratio is deteriorated with the changes in the W_{s1} or W_{s2}. With the $\pm$ 10 nm changes in both the W_{s1} and W_{s2}, the deterioration of the splitting ratio (O_2/O_1) is less than 5.46% with values remaining between 89.88% and 84.42%. However, the fabrication errors can be further compensated by utilizing the TO effect by implementing micro-heaters upon the phase-shifting sections.

III. CONCLUSION

In conclusion, we have proposed a concept of power splitter with selectable splitting-ratios based on two MMI sections connected by a phase-shifting region. As an example, an asymmetrical power splitter (10 : 90) via cascaded 1×10 and 9×1 MMI couplers is optimized, in which phase-matching conditions can be met by utilizing a simple angled structure or alternatively using the phase shifters between two cascaded couplers. The proposed splitters have been optimized by using the TMM and 3D-FV-BPM. The simulated results show that an angled MMI-coupler based splitter is with an insertion loss of 0.74 dB and a total length of 192 μm at angle, $\theta = 1.2°$. Furthermore, a more compact splitter with a length of 58 μm and an insertion loss of only 0.41 dB was achieved based on CMMIs. For $\pm$ 10 nm changes in W_{s1} and W_{s2}, the resulting insertion-loss deterioration was less than 0.164 dB and splitting ratio change of 5.46%. Although, in this paper, the proposed splitter is only designed for the quasi-TE polarization, but an asymmetrical power splitter for the quasi-TM mode or even polarization independent splitter can also be developed by considering the similar configurations.

REFERENCES

[1] P. P. Absil, P. Verheyen, P. D. Heyn, M. Pantouvaki, G. Lepage, J. D. Coster, and J. V. Campenhout, "Silicon photonics integrated circuits: a manufacturing platform for high density, low power optical I/O's," *Opt. Express,* vol. 23, no. 7, pp. 9369-9378, Apr. 2015.

[2] A. B. Khanikaev and A. Alù, "Silicon photonics: One-way photons in silicon," *Nat. Photonics*, vol. 8, no. 9, pp. 680-682, Sep. 2014.

[3] Y. Wang, S. Gao, K. Wang, and E. Skafidas, "Ultra-broadband and low-loss 3 dB optical power splitter based on adiabatic tapered silicon waveguides," *Opt. Lett.*, vol. 41, no. 9, pp. 2053-2056, Apr. 2016.

[4] H. Xu and Y. Shi, "Ultra-broadband dual-mode 3 dB power splitter based on a Y-junction assisted with mode converters," *Opt. Lett.*, vol. 41, no. 21, pp. 5047-5050, Nov. 2016.

[5] U. Koren, B. I. Miller, M. G. Young, M. Chien, K. Dreyer, R. Ben-Michael, and R. J. Capik, "A 1.3-μm wavelength laser with an integrated output power monitor using a directional coupler optical power tap," *IEEE Photon. Technol. Lett.*, vol. 8, no. 3, pp. 364-366, Mar. 1996.

[6] A. R. Gupta, K. Tsutsumi, and J. Nakayama, "Synthesis of hadamard

transformers by use of multimode interference optical waveguides," *Appl. Opt.*, vol. 42, no. 15, pp. 2730-2738, May 2003.

[7] D. T. Spencer, D. Dai, Y. Tang, M. J. Heck, and J. E. Bowers, "Realization of a novel power splitter with uniformly excited ports," *IEEE Photon. Technol. Lett.*, vol. 25, no. 1, pp. 36-39, Jan. 2013.

[8] H. Yi, Q. Long, W. Tan, L. Li, X. Wang, and Z. Zhou, "Demonstration of low power penalty of silicon Mach-Zehnder modulator in long-haul transmission," *Opt. Express*, vol. 20, no. 25, pp. 27562-27568, Dec. 2012.

[9] S. Matsuo, Y. Yoshikuni, T. Segawa, Y. Ohiso, and H. Okamoto, "A widely tunable optical filter using ladder-type structure," *IEEE Photon. Technol. Lett.*, vol. 15, no. 8, pp. 1114-1116, Aug. 2003.

[10] X. Tang, J. Liao, H. Li, L. Zhang, R. Lu, and Y. Liu, "A novel scheme for 1 × N optical power splitter," *Opt. Express*, vol. 18, no. 21, pp. 21697-21704, Oct. 2010.

[11] K. S. Reichel, R. Mendis, and D. M. Mittleman, "A broadband terahertz waveguide T-junction variable power splitter," *Sci. Rep.*, vol. 6, pp. 28925, Jun. 2016.

[12] D. C. Tee, N. Tamchek, Y. G. Shee, and F. M. Adikan, "Numerical investigation on cascaded 1 × 3 photonic crystal power splitter based on asymmetric and symmetric 1 × 2 photonic crystal splitters designed with flexible structural defects," *Opt. Express*, vol. 22, no. 20, pp. 24241-24255, Oct. 2014.

[13] N. S. Mohamed-Kassim, A. B. M. Ibrahim, and M. K. Abd-Rahman, "Low loss and dynamically tunable power splitter based on circular-to-rectangular POF converter," *J. Lightwave Technol.*, vol. 34, no. 4, pp. 1306-1312, Feb. 2016.

[14] N. S. Lagali, M. R. Paiam, and R. I. MacDonald, "Theory of variable-ratio power splitters using multimode interference couplers," *IEEE Photon. Technol. Lett.*, vol. 11, no. 6, pp. 665-667, Jun. 1999.

[15] Z. Lu, H. Yun, Y. Wang, Z. Chen, F. Zhang, N. A. Jaeger, and L. Chrostowski, "Broadband silicon photonic directional coupler using asymmetric-waveguide based phase control," *Opt. Express*, vol. 23, no. 3, pp. 3795-3808, Feb. 2015.

[16] H. Subbaraman, X. Xu, A. Hosseini, X. Zhang, Y. Zhang, D. Kwong, and R. T. Chen, "Recent advances in silicon-based passive and active optical interconnects," *Opt. Express*, vol. 23, no. 3, pp. 2487-2510, Feb. 2015.

[17] J. Leuthold and C. H. Joyner, "Multimode interference couplers with tunable power splitting ratios," *J. Lightwave Technol.*, vol. 19, no. 5, pp. 700-707, May 2001.

[18] D. J. Y. Feng, P. Y. Chang, T. S. Lay, and T. Y. Chang, "Novel stepped-width design concept for compact multimode-interference couplers with low cross-coupling ratio," *IEEE Photon. Technol. Lett.*, vol. 19, no. 4, pp. 224-226, Mar. 2007.

[19] J. D. Doménech, J. S. Fandiño, B. Gargallo, and P. Muñoz, "Arbitrary Coupling ratio multimode interference couplers in Silicon-on-Insulator," *J. Lightwave Technol.*, vol. 32, no. 14, pp. 2536-2543, Jul. 2014.

[20] Q. Lai, M. Bachmann, W. Hunziker, P. A. Besse, and H. Melchior, "Arbitrary ratio power splitters using angled silica on silicon multimode interference couplers," *Electron. Lett.*, vol. 32, no. 17, pp. 1576-1577 Aug. 1996.

[21] M. Bachmann, P. A. Besse, and H. Melchior, "Overlapping-image multimode interference couplers with a reduced number of self-images for uniform and nonuniform power splitting," *Appl. Opt.*, vol. 34, no. 30, pp. 6898-6910, Oct. 1995.

[22] Q. Deng, L. Liu, X. Li, and Z. Zhou, "Arbitrary-ratio 1 × 2 power splitter based on asymmetric multimode interference," *Opt. Lett.*, vol. 39, no. 19, pp. 5590-5593, Oct. 2014.

[23] D. A. May-Arrioja, P. LiKamWa, C. Velásquez-Ordóñez, and J. J. Sánchez-Mondragón, "Tunable multimode interference coupler," *Electron. Lett.*, vol. 43, no. 13, pp. 1-2, Jul. 2007.

[24] X. Wu, L. Liu, Y. Zhang, D. Li, W. Wang, and L. Xu, "Low electric power driven thermo-optic multimode interference switches with tapered heating electrodes," *Opt. Commun.*, vol. 258, no. 2, pp. 135-143, Feb. 2006.

[25] H. S. Chu, P. Bai, E. P. Li, and W. R. J. Hoefer, "Hybrid dielectric-loaded plasmonic waveguide-based power splitter and ring resonator: compact size and high optical performance for nanophotonic circuits," *Plasmonics*, vol. 6, no. 3, pp. 591-597, Sep. 2011.

[26] P. A. Besse, E. Gini, M. Bachmann, and H. Melchior, "New 2 × 2 and 1 × 3 multimode interference couplers with free selection of power splitting ratios," *J. Lightwave Technol.*, vol. 14, no. 10, pp. 2286-2293, Oct. 1996.

[27] Y. Jiao, P. Chen, J. Hu, and Y. Shi, "Experimental demonstration of bending multimode interference couplers for arbitrary power splitting," *Electron. Lett.*, vol. 46, no. 8, pp. 583-584, Apr. 2010.

[28] J. Zhang, L. Han, B. P. Kuo, and S. Radic, "Arbitrary ratio, wavelength-insensitive 2 × 2 MMI coupler in SOI with enhanced fabrication tolerance,"

in *CLEO: Science and Innovations*, San Jose, 2018, pp. STh4A-8.

[29] A. Zanzi, A. Brimont, A. Griol, P. Sanchis, and J. Marti, "Compact and low-loss asymmetrical multimode interference splitter for power monitoring applications," *Opt. Lett.*, vol. 41, no. 2, pp. 227-229, Jan. 2016.

[30] J. Leuthold, J. Eckner, E. Gamper, and P. A. Besse, "Multimode interference couplers for the conversion and combining of zero- and first-order modes," *J. Lightwave Technol.*, vol. 16, no. 7, pp. 1228-1239, Jul. 1998.

[31] R. Thapliya, T. Kikuchi, and S. Nakamura, "Tunable power splitter based on an electro-optic multimode interference device," *Appl. Opt.*, vol. 46, no. 19, pp. 4155-4161, Jul. 2007.

[32] J. Wang, X. Guan, Y. He, Y. Shi, Z. Wang, S. He, P. Holmström, L. Wosinski, L. Thylen, and D. Dai, "Sub-μm² power splitters by using silicon hybrid plasmonic waveguides," *Opt. Express*, vol. 19, no. 2, pp. 838-47, Jan. 2011.

[33] D. S. Levy, R. Scarmozzino, Y. M. Li, and R. M. Osgood, "A new design for ultracompact multimode interference-based 2 × 2 couplers," *IEEE Photon. Technol. Lett.*, vol. 10, no. 1, pp. 96-98, Jan. 1998.

[34] D. S. Levy, Y. M. Li, R. Scarmozzino, and R. M. Osgood, "A multimode interference-based variable power splitter in GaAs-AlGaAs," *IEEE Photon. Technol. Lett.*, vol. 9, no. 10, pp. 1373-1375, Oct. 1997.

[35] C. D. Truong and T. T. Le, "Power splitting ratio couplers based on mmi structures with high bandwidth and large tolerance using silicon waveguides," *Photon. Nanostruct.*, vol. 11, no. 3, pp. 217-225, Aug. 2013.

[36] D. J. Y. Feng, T. S. Lay, and T. Y. Chang, "Waveguide couplers with new power splitting ratios made possible by cascading of short multimode interference sections," *Opt. Express*, vol. 15, no. 4, pp. 1588-1593, Feb. 2007.

[37] N. S. Lagali, M. R. Paiam, R. I. Macdonald, K. Rhoff, and A. Driessen, "Analysis of generalized mach-zehnder interferometers for variable-ratio power splitting and optimized switching," *J. Lightwave Technol.*, vol. 17, no. 12, pp. 2542-2550, Dec. 1999.

[38] D. J. Feng and T. S. Lay, "Compact multimode interference couplers with arbitrary power splitting ratio," *Opt. Express*, vol. 16, no. 10, pp. 7175-7180, May 2008.

[39] T. T. Le, L. W. Cahill, and D. M. Elton, "Design of 2 × 2 SOI MMI couplers with arbitrary power coupling ratios," *Electron. Lett.*, vol. 45, no. 22, pp. 1118-1119, Oct. 2009.

[40] M. Cherchi, S. Ylinen, M. Harjanne, M. Kapulainen, T. Vehmas, and T. Aalto, "Unconstrained splitting ratios in compact double-MMI couplers," *Opt. Express*, vol. 22, no. 8, pp. 9245-9253, Apr. 2014.

[41] L. B. Soldano and E. C. M. Pennings, "Optical multi-mode interference devices based on self-imaging: principles and applications," *J. Lightwave Technol.*, vol. 13, no. 4, pp. 615-627, Apr. 1995.

Weifeng Jiang received PhD degree in Physics Electronics from Southeast University, Nanjing, China, in 2015. He has been in City, University of London as a postdoctoral fellow from Aug. 2015 to Oct. 2016. In 2017, he joined Nanjing University of Posts and Telecommunications, as a lecturer. He is working on silicon photonics for optical communications and sensing.

B. M. Azizur Rahman received the B.Sc.Eng and M.Sc.Eng. degrees in Electrical Engineering with distinctions from Bangladesh University of Engineering and Technology (BUET), Dhaka, Bangladesh, in 1976 and 1979, respectively. He also received two gold medals for being the best undergraduate and graduate students of the university in 1976 and 1979, respectively. In 1979, he was awarded with a Commonwealth Scholarship to study for a PhD degree in the UK and subsequently in 1982 received his PhD degree in Electronics from University College London.

In 1988, he joined City University, London, as a lecturer, where became a full Professor in 2000. At City University, he leads the research group on Photonics Modelling, specialised in the development and use of rigorous and full-vectorial numerical approaches to design, analyse and optimise a wide range of photonic devices, such as spot-size converters, high-speed optical modulators, compact bend designs, power splitters, polarisation splitters, polarisation rotators, polarization controllers, SBS, terahertz devices, etc. He has published more than 550 journal and conference papers, and his journal papers have been cited more than 4500 times. He has supervised 29 students to complete their PhD degrees as their first supervisor and received more than £11 M in research grants. Prof. Rahman is Fellow of the IEEE, Optical Society of America and the SPIE.